Integrated discharge scenario for high-temperature helical plasma in LHD

2015 Nucl. Fusion 55 113020

(http://iopscience.iop.org/0029-5515/55/11/113020)

OPEN ACCESS
IOP Publishing | International Atomic Energy Agency
Nuclear Fusion
Nucl. Fusion **55** (2015) 113020 (8pp)
doi:10.1088/0029-5515/55/11/113020

Integrated discharge scenario for high-temperature helical plasma in LHD

K. Nagaoka[1,2], H. Takahashi[1], S. Murakami[3], H. Nakano[1], Y. Takeiri[1,2], H. Tsuchiya[1], M. Osakabe[1], K. Ida[1,2], M. Yokoyama[1], M. Yoshinuma[1], S. Morita[1,2], M. Goto[1,2], T. Oishi[1,2], N. Pablant[4], K. Fujii[5], K. Tanaka[1], N. Tamura[1], Y. Nakamura[1,2], X. Du[2], T. Ido[1], A. Shimizu[1], S. Kubo[1], H. Igami[1], R. Seki[1], C. Suzuki[1], Y. Suzuki[1,2], K. Tsumori[1,2], K. Ikeda[1], M. Kisaki[1], Y. Yoshimura[1], T. Shimozuma[1], T. Seki[1], K. Saito[1], H. Kasahara[1], S. Kamio[1], T. Mutoh[1,2], O. Kaneko[1,2], H. Yamada[1,2], A. Komori[1,2] and the LHD Experiment Group

[1] National Institute for Fusion Science, Toki, 509–5292, Japan
[2] SOKENDAI (Graduate School for Advanced Studies), Toki 509–5292, Japan
[3] Department of Nuclear Engineering, Kyoto University, Kyoto 606–8501, Japan
[4] Princeton Plasma Physics Laboratory, Princeton, New Jersey 08543, USA
[5] Department of Mechanical Engineering and Science, Kyoto University, Kyoto 615–8540, Japan

E-mail: nagaoka@nifs.ac.jp

Received 2 February 2015, revised 23 July 2015
Accepted for publication 18 August 2015
Published 28 September 2015

Abstract

The discharge scenario of high temperature plasma with a helical configuration has significantly progressed. The increase of central ion temperature due to the reduction of wall recycling was clearly observed. The peaking of the ion heating profile and the reduction of charge exchange loss of energetic ions play an important role for further improvement of ion heat transport in the ion internal transport barrier (ITB) core. The ion ITB and electron ITB have been successfully integrated due to the superposition of centrally focused electron cyclotron heating to the ion ITB plasma, and the high temperature regime of the ion temperature comparable to the electron temperature ($T_i \sim T_e$) has been significantly extended. The width of the ion ITB formed with electron ITB is wider than the width of electron ITB. The positive radial electric field was observed in the integrated ITB plasma by a heavy ion beam probe, while the negative radial electric field was observed in ion ITB plasmas. The ion temperature gradient decreases with the increase of the temperature ratio (T_e/T_i).

Keywords: helical plasma, ITB, discharge scenario, impurity hole, radial electric field

(Some figures may appear in colour only in the online journal)

1. Introduction

Discharge scenario development for high-temperature plasmas is a crucial issue for realizing helical reactors, because it has been confirmed that helical plasmas have good confinement properties in the high density regime and a significant advantage in the steady state operation. High electron temperature helical plasma had been obtained with the electron internal transport barrier (ITB)/ core electron root confinement (CERC) in many devices [1–6]. The electron ITB forms with centrally focused electron cyclotron heating (ECH) in the core region. The transport improvement is characterized by the suppression of anomalous transport as well as neoclassical transport due to the transition of the radial electric field. The contribution of zonal flow to the turbulence suppression has also been identified experimentally [7].

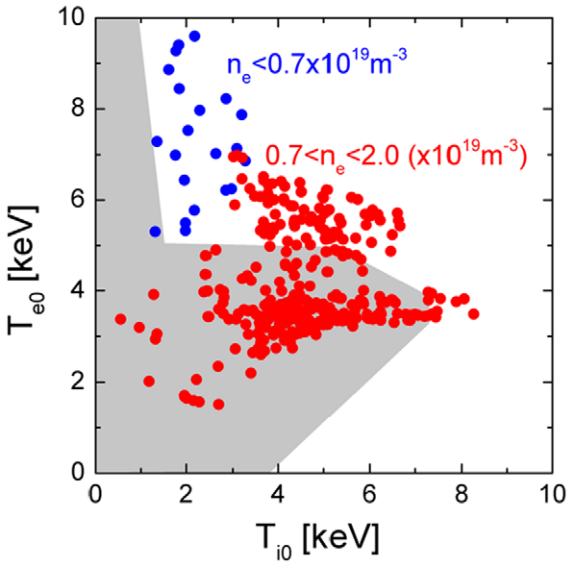

Figure 1. The parameter regime of high temperature plasma in the LHD. The hatched area indicates the achieved region until the 2013 experiment campaign in the LHD.

On the other hand, high ion temperature helical plasmas have been obtained with ion ITB formation and have been intensively studied in the large helical device (LHD) [8–11]. The basic characteristics of heat transport have gyro-Bohm dependence in the normal confinement of LHD plasmas. The ITB is defined by the transport improvement from gyro–Bohm dependence and the normalized temperature gradient ($R/L_T = -(R/T)$ * grad$T$) is a useful measure to identify ITB formation [8, 12]. The ion ITB forms in neutral beam injection (NBI) heated plasma with a low recycling wall condition. The reduction of anomalous transport to the neoclassical transport level has been identified in the LHD experiment [10]. The weak negative radial electric field is formed in ion ITB core plasma and no transition of the radial electric field is observed associated with the ion ITB formation. The mechanism of suppression of anomalous transport and contribution of wall recycling to the ion heat transport in the core are not yet fully understood. Moreover, the ion ITB and electron ITB have been observed separately in the helical plasmas in contrast to the tokamak ITB plasmas, indicating that the coupling between ion and electron heat transport is much weaker than those of tokamak plasmas.

Recently, discharge scenarios of ion ITB and electron ITB have been integrated in the LHD, and the high temperature regime of helical plasma has been significantly extended in the region of the ion temperature comparable to the electron temperature ($T_i \sim T_e$), which is summarized in figure 1. The high ion temperature regime has been also extended in the LHD due to intensive wall conditioning, and the central ion temperature of 8.1 keV has been achieved, which is the new record of helical plasmas with the low Z_{eff} ($= \sum(z_j^2 n_j / z_j n_j)$) condition.

In this paper, the discharge scenario of ion ITB is presented, and the mechanism of wall conditioning effects on the ion heat transport in the core is discussed in the next section. The simultaneous formation of ion and electron ITBs is described. The dependence of temperature ratio (T_e/T_i) on the ion heat transport is discussed in section 3. The impact of this study is discussed in the summary from the viewpoint of reliable reactor design.

2. Discharge scenario of the ion ITB

The stage for this study is the LHD, which is the world's largest helical plasma device. The major radius and the minor radius are 3.9 m and 0.6 m, respectively. The plasmas were heated with tangential negative-ion-based NBIs (negative NBIs) with a very high beam energy up to 190 keV and total port-through power of 16 MW. The perpendicular positive-ion-based NBIs (positive NBIs) with low beam energy around 40 keV and total port-through power of 12 MW were also injected for high power ion heating experiments in the LHD. The one beam line of perpendicular NBI operates the beam injection with the modulation technique (ON/OFF = 80 ms/20 ms) to calibrate the background signal for ion temperature measurement with charge exchange spectroscopy [13].

2.1. Ion ITB formation

Ion ITB forms in the core of NBI heated plasmas. These discharges were obtained after intensive wall conditioning main discharges [14]. Figure 2 shows a typical discharge with ion ITB formation. The three negative NBIs were superposed to positive NBI heated plasma at $t = 4.74$ s. The helium gas puff was operated in the initial phase of the discharge to control the plasma density. A carbon pellet with the cylindrical shape (diameter: $\phi = 1.0$ mm and length: $l = 1.0$ mm) was injected, and the plasma density then increased. The additional positive NBI started the beam injection just after the carbon pellet injection. The ion temperature increased and ion ITB formed in the density decay phase after the carbon pellet injection. The radial profile of the ion ITB plasma is shown in figure 2(d). The peaked ion temperature profile with a steep gradient was observed in the core region. The central ion temperature (T_{i0}) of 8.1 keV was observed. No ITB was observed in the electron temperature and electron density profiles.

The ion heat transport was analyzed, in which the dynamic time evolution of the plasma parameters are taken into account. The ion thermal diffusivity decreases with the factor of 3–5 and reaches the neoclassical transport level, indicating that the anomalous transport is significantly suppressed at the barrier position [10]. The negative radial electric field (E_r) was evaluated by the electrostatic potential profile measurement with a heavy ion beam probe (HIBP) [15].

The density profile is almost flat in the core, indicating no transport barrier in particle transport. The outward convection of impurity was observed in the formation of ion ITB, and the extremely hollow profile of impurity, the so-called 'impurity hole' [16, 17], was formed when the ion temperature gradient became large, which is shown in figure 2(e). The dynamics of impurity transport associated with the ion ITB formation is discussed in another paper [18], and the mechanism of the

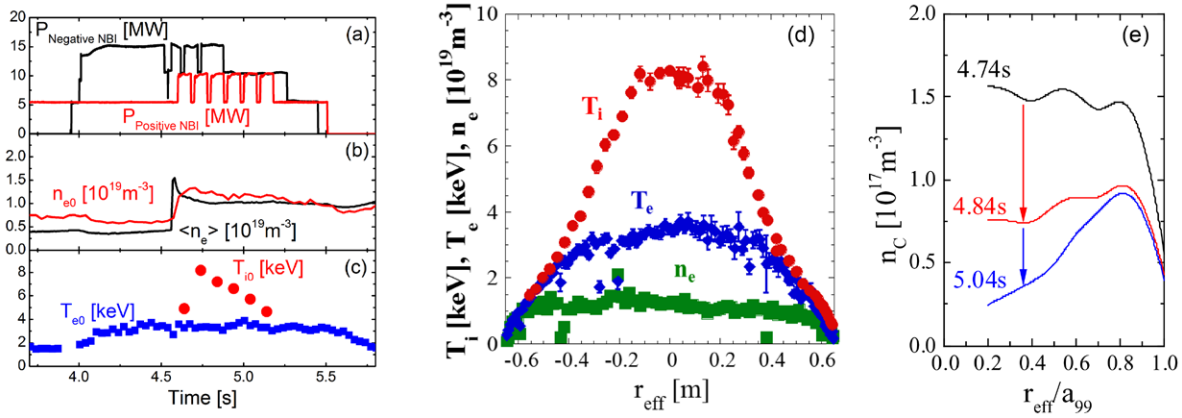

Figure 2. Typical wave form of (*a*) port-through power of negative NBI (tangential injection) and positive NBI (perpendicular injection), (*b*) central electron density (n_{e0}) and line averaged electron density ($<n_e>$), and (*c*) ion and electron temperatures at the center of ion ITB plasma (T_{i0} and T_{e0}, respectively). (*d*) Profiles of (red) the ion temperature, (blue) the electron temperature and (green) the electron density at $t = 4.74$ s. (*e*) The time evolution of the carbon density profile (n_C). The extremely hollow impurity profile (impurity hole) was formed in the ion ITB plasma. The r_{eff} is the averaged minor radius on a magnetic flux surface, and the a_{99} is the effective minor radius in which 99% of the plasma kinetic energy is confined and is 0.614 m in this plasma.

impurity hole formation remains an open question. It is noted that impurity accumulation has never been observed to be associated with the ion ITB formation in helical plasmas in contradiction to the tokamak ITB plasmas [19].

The ion ITB was observed to degrade the performance after the central ion temperature reached the maximum value. The time evolution of the ion ITB formation and back transition were analyzed with TASK-3D and GNET codes. The time scale of the degradation is the order of the slowing down time of the beam ions originated with NBI. However, the amplitude of the degradation cannot be explained by the reduction of heating power [20]. It was also pointed out that the carbon impurity content may play some roles in the improvement of ion heat transport [21].

2.2. Effects of wall conditioning

The ion temperature was observed to increase with wall conditioning. The repetitive long pulse helium discharges were observed to be effective for the reduction of wall recycling and for the increase of the central ion temperature (strong ITB formation) in LHD. Figure 3(*a*) shows the time evolution of hydrogen gas pressure in the vacuum vessel. The hydrogen pressure continued to decrease during repetitive helium discharge with ion cyclotron range of frequency heating (ICH) and to increase during the repetitive ion ITB discharges. The higher ion temperature plasma was obtained with lower hydrogen pressure conditions, which is shown in figures 3(*b*) and (*c*). However, the linkage between the reduction of wall recycling and the ion heat transport in the core has long been an open question. Here we compare weak ITB and strong ITB formed before and after repetitive helium conditioning discharges, respectively, and discuss the helium conditioning effects on the strength of the ITB formation.

The change of density profile was observed between the weak ITB plasma and the strong ITB plasma as shown in figure 3(*d*). The electron density (n_e) near the edge is significantly reduced for the strong ITB plasma. The beam deposition profiles of the NBIs and the profile of ion heating power were calculated with the FIT-3D code. The profiles of ion heat flux density (Q_i) are compared between weak and strong ITBs (figure 3(*e*)). The ratio of the ion heating power deposited inside of the half radius (defined as $Q_i(r_{eff}/a_{99} = 0.5) * S_{0.5}/Q_i(r_{eff}/a_{99} = 1.0) * S_{1.0}$, where r_{eff} is the averaged minor radius on a magnetic flux surface, and a_{99} is the effective minor radius in which 99% of the plasma kinetic energy is confined. $S_{0.5}$ and $S_{1.0}$ are the area of magnetic flux surface at $r_{eff}/a_{99} = 0.5$ and $r_{eff}/a_{99} = 1.0$, respectively) is 0.48 for the weak ITB plasma and is 0.55 for the strong ITB plasmas, indicating that the ion heating power profile becomes more peaked after the helium discharges.

In order to investigate charge exchange loss effect in the core, the neutral particle density was measured with a high-dynamic range of Balmer-α spectroscopy [22, 23], which was newly installed in LHD. The reduction of neutral particles with a factor of three was observed even in the core after the repetitive helium conditioning discharges. The beam slowing down spectra were calculated using averaged values inside the half radius, and the charge exchange loss effect appears in the low energy range less than 50 keV. The charge-exchange loss of energetic ions was evaluated for the tangential NBI of which beam energy is 180 keV. The charge exchange loss without wall conditioning was 14% in ion heating power before wall conditioning, and it was reduced to 7% after the wall conditioning.

The increase of the heating power in the ion ITB core region is attributed to the effects of the change of the density profile and reduction of charge exchange loss of energetic ions. Figure 4 shows the comparison of flux-gradient relation of the developing phase of ion ITB. The change of charge exchange loss of fast ions is taken into account in the analysis. The both the weak and the strong ITBs formed passing through almost the same region in the flux-gradient relation. The achieved maximum ion temperature gradient for the strong ITB plasma is 1.8 times larger than that for the weak ITB plasma, while the difference of heat flux between the strong and the weak

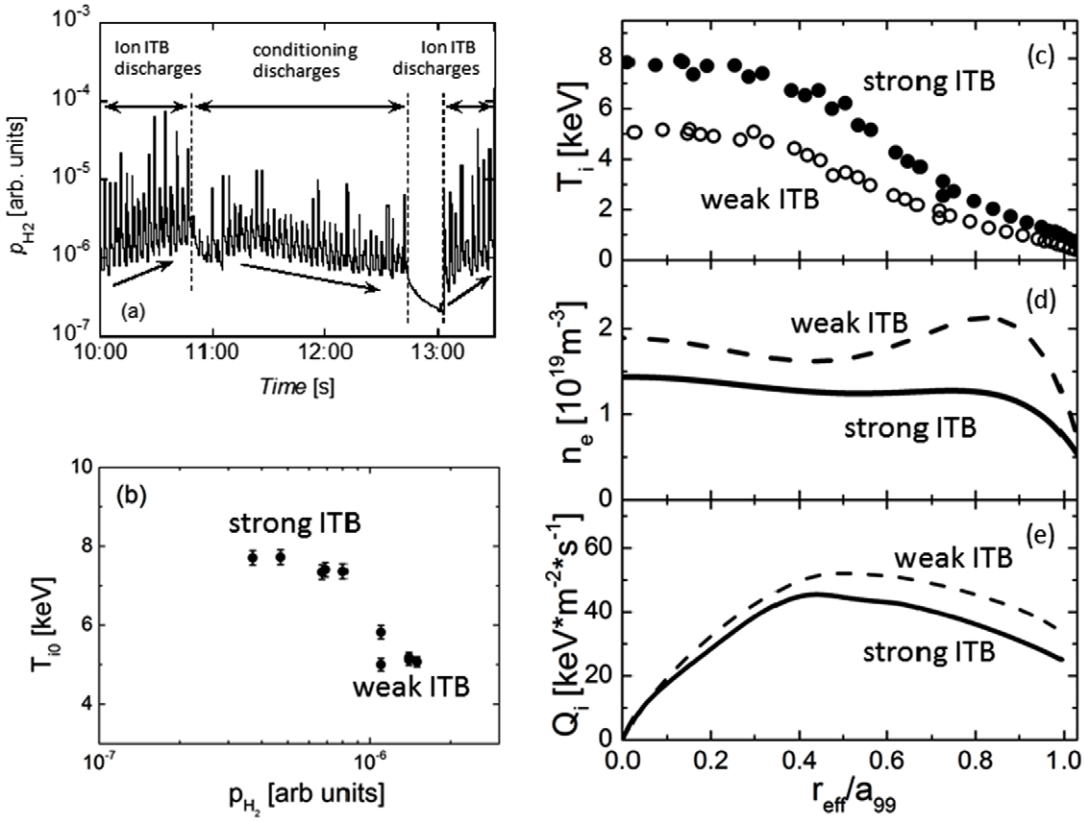

Figure 3. (*a*) The time evolution of hydrogen partial pressure. (*b*) The achieved central ion temperature (T_{i0}) as a function of residual hydrogen gas pressure just before the discharges. The high-ion-temperature plasma was produced by the formation of strong ITB in the low residual hydrogen pressure condition. (*c*) The ion temperature profiles, (*d*) the density profiles and (*e*) the ion heat flux profile as a function of r_{eff}/a_{99}.

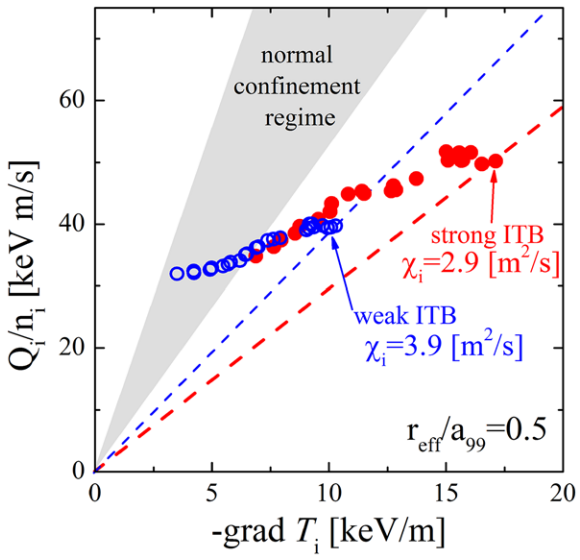

Figure 4. Flux-gradient relation of heat transport at $r_{eff}/a_{99} = 0.5$. The Q_i is a heat flux density and the n_i is an ion density composed of hydrogen ions and helium ions ($n_i = n_H + n_{He}$). The dashed lines indicate the thermal diffusivity ($\chi_i = -Q_i/n_i$ grad T_i) of $\chi_i = 3.9$ [m^2 s^{-1}] (blue) and $\chi_i = 2.9$ [m^2 s^{-1}] (red). The hatched area indicates the region of normal confinement plasmas.

ITB plasma is within a factor of 1.3. This causes the further reduction of effective ion thermal diffusivity, χ_i ($=-Q_i/n_i$ grad T_i), where the ion density (n_i) is the total ion density (sum of hydrogen ion density and helium ion density) evaluated with visible spectroscopy data. The ion density ratio (n_i / n_e) is 0.64 for the strong ITB plasma and 0.67 for the weal ITB plasma. The achieved minimum value of effective ion thermal diffusivity is $\chi_i = 3.9$ (m^2 s^{-1}) for the weal ITB plasma and $\chi_i = 2.9$ (m^2 s^{-1}) for the strong ITB plasma. It is noted that the heat transport (χ_i) of ion ITB plasmas improves further when the heat flux increases. The improvement of ion heat transport makes the wall conditioning much more effective in increasing the central ion temperature although the increase of direct ion heating power is not so significant, being of the order of 10%. It is also noted that no saturation of the ion temperature gradient was observed in the flux-gradient relation in the present experiment in LHD.

3. Integration of ion ITB and electron ITB

In the LHD experiment campaign in 2012, the ECH power capability was increased up to 4.6 MW and the density regime of electron ITB formation with the central electron temperature over 10 keV increased to the same regime with ion ITB [24], which has enabled the integration of ion and electron ITBs in the experiment campaign in 2013. An electron ITB and an ion ITB were successfully combined due to the application of centrally focused ECH, and the temperature regime of helical plasma with $T_i \sim T_e$ was significantly extended (see figure 1).

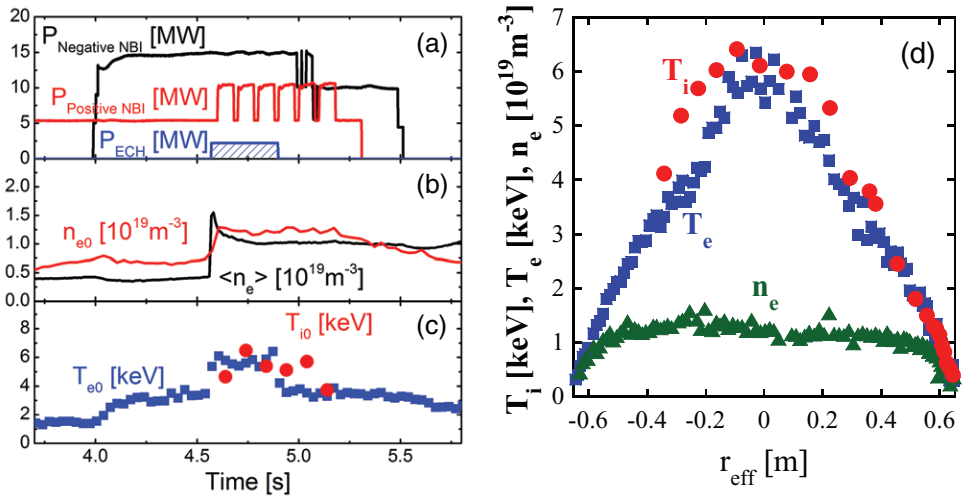

Figure 5. Time evolution of (*a*) port-through heating power of positive NBI (perpendicular injection to the magnetic axis), negative NBI (tangential injection) and ECH, (*b*) the central electron density (n_{e0}) and the line averaged electron density ($<n_e>$), and (*c*) ion and electron temperatures at the center (T_{i0} and T_{e0}, respectively). (*d*) The radial profile of ion temperature, electron temperature, and electron density at $t = 4.74$ s.

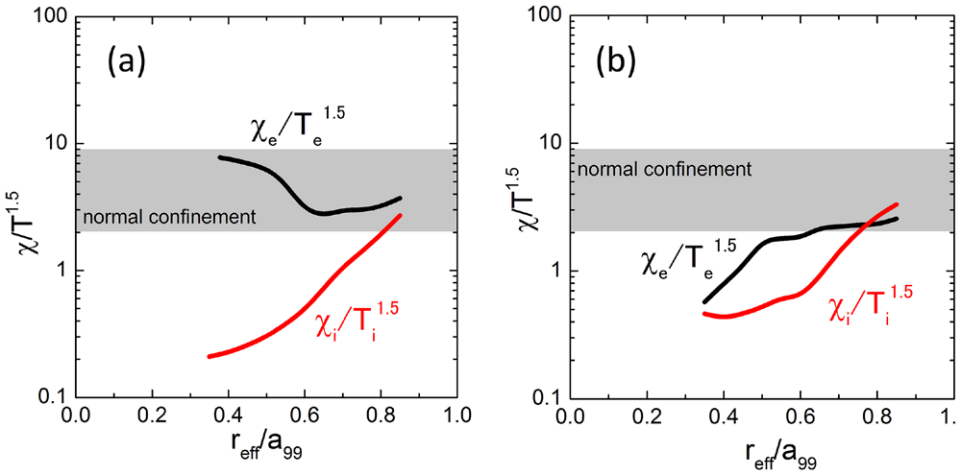

Figure 6. Radial profile of thermal diffusivity normalized by gyro-Bohm temperature dependence ($\chi_{i,e}/T_{i,e}^{1.5} = -Q_{i,e}/n_{i,e}$ grad $T_{i,e}$) of (*a*) ion ITB plasma shown in figure 2 ($t = 4.74$ s) and (*b*) ion and electron ITBs plasma shown in figure 5 ($t = 4.74$ s). The red and black curves show the ion and electron thermal diffusivity, respectively.

Figures 5(*a*)–(*c*) show a typical wave form with simultaneous formation of ion and electron ITBs with the low wall recycling condition. The centrally focused ECH was applied to NBI heated plasma, the electron temperature then increased over 6 keV. The carbon pellet was injected into the plasma, and another perpendicular NBI started the beam injection just after carbon pellet injection. The ion temperature increases in a similar way with the ion ITB formation shown in figure 2(*a*). Figure 5(*d*) shows the radial profiles of temperatures and density of the plasma with $T_{i0} \sim T_{e0} \sim 6$ keV. The steep gradient of ion and electron temperatures was observed to be formed, and the density profile is almost flat in the core. The normalized temperature gradient of the ion and electron temperature gradient ($R/L_{Ti,e} = -(R/T_{i,e})(dT_{i,e}/dr_{eff})$, where R is major radius of the magnetic axis, and $T_{i,e}$ is temperature of ion/ electron.) is a good measure for identification of ITB [25] because the profile stiffness caused by a gyro-Bohm dependence of heat transport is broken when ITB is formed. The normalized temperature gradient at the steep gradient for ion and electron are both over 10, while they are 3–8 in the normal confinement, indicating that the ion and electron ITBs are formed simultaneously. It is noted that the width of ion ITB is wider than that of electron ITB in contradiction to tokamak ITB plasmas.

The heat transport was calculated with the TASK-3D code [26, 27]. The time evolution of the plasma parameters and beam slowing down were taken into account. Figure 6 shows ion and electron thermal diffusivities normalized by the gyro-Bohm temperature dependence ($\chi_{i,e}/T_{i,e}^{1.5} = -(-Q_{i,e}/n_{i,e}$ grad $T_{i,e})/T_{i,e}^{1.5}$) for (a) ion ITB shown in figure 2(*b*) integrated ITB discharge shown in figure 5. In the integrated ITB plasma, the ECH power of 2.2 MW is deposited locally at the normalized minor radius of $r_{eff}/a_{99} < 0.15$, which is almost one-third of the total electron heating power because the main power of negative NBI is absorbed by electrons due to the large beam

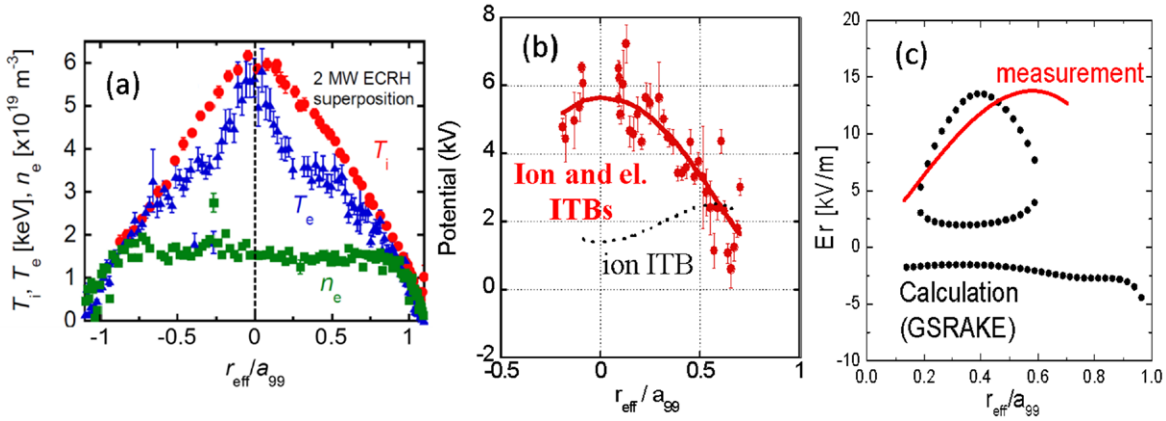

Figure 7. (*a*) The profile of ion and electron temperatures and electron density of the plasma with ITBs formation with the magnetic field of $B_t = +2.75$ T, in which a heavy ion beam probe (HIBP) is available to measure the electrostatic potential profile. (*b*) The electrostatic potential profile measured with HIBP. (*c*) Profile of the radial electric field obtained by experimental measurement (red curve) and neoclassical calculation (black circles).

energy up to 190 keV. In the case of ion ITB, the ion heat transport improved in the core region, and no improvement was observed in electron transport. On the other hand, in the case of integrated ITB plasma, the transport improvement was confirmed in both the ion and electron transport in the core. It is noted that the ITB foot was clearly observed to be located at different radial positions between the ion ITB and the electron ITB, suggesting that the physics mechanism of transport improvement is not identical between ion and electron transport.

The profile of electrostatic potential was measured with the heavy ion beam probe (HIBP). Figures 7(*a*) and (*b*) show the radial profile of plasma parameters and the electrostatic potential measured with HIBP, respectively. A peaked potential profile corresponding to the positive radial electric field ($E_r \sim 8\,\mathrm{kV\ m^{-1}}$) is observed during the formation of ion and electron ITBs. In contradiction to this observation, it was observed in a previous study that the ion ITB without ECH was formed with negative radial electric field, which is shown by the dashed line in figure 7(*b*) [10]. The ambipolar radial electric field was calculated by neoclassical transport code (GSRAKE) [28] and was compared with the experimental observation, which is shown in figure 7(*c*). There are three branches in the core region. The upper branch is an electron root and the bottom branch is an ion root. The middle branch is an unstable one and is not realistic. The experimental observation agrees well with the E_r in the electron root branch, indicating that the ion heat transport in the core may be also improved with a positive electric field.

In previous research on CERC, ion ITB had never formed with positive Er. The reason is considered to be that the ion heating power is too low and the electron density is much less than that of ion ITB plasma. This is the first observation of improvement of ion heat transport in the core with positive values of Er. However, the transport improvement does not seem to correlate with positive Er formation, because the radial position of the barriers are different between ion ITB and electron ITB, suggesting the contribution of improvement of anomalous transport in the ion heat transport.

In order to investigate the characteristics of improved transport for ion and electron ITB plasmas, here we discuss the normalized temperature gradient (R/L_T) at the transport barrier ($r_{eff}/a_{99} = 0.45$) with a dataset obtained in the density regime from $0.3 \times 10^{19}\mathrm{m^{-3}}$ to $2 \times 10^{19}\mathrm{m^{-3}}$. The central ion and electron temperatures of this dataset are shown in figures 8(*a*) and (*b*), respectively. The density dependence of ion temperature is different from that of electron temperature, in particular, in the low density regime less than $0.7 \times 10^{19}\mathrm{m^{-3}}$. The density dependence and temperature ratio dependence of the R/L_T are shown in figures 8(*c*)–(*f*). The R/L_{Ti} decreases in the low density regime, while no change is observed in R/L_{Te}. The R/L_{Ti} is also observed to decrease with local temperature ratio (T_e/T_i), while the R/L_{Te} does not change with T_e/T_i. In particular, the strong ion ITB forms only in the region of $T_e/T_i < 1$. This temperature ratio dependence is consistent with the observed difference in ITB width. In the LHD experiment, the width of electron ITB changes depending on island formation at the rational surface, iota profile (profile of NB-driven current), etc. The width of ion ITB also changes depending on some parameters such as iota profile, electron density and carbon density. However, in the present experiment, observed was only the combination of wider ion ITB and narrower electron ITB. The reason for the combination of narrower ion ITB and wider electron ITB was not observed, but may be understood by the temperature ratio dependence of ion heat transport. The ion heat transport degrades with T_e/T_i in the region of $T_e/T_i > 1$.

4. Discussion and summary

The development of a discharge scenario for high temperature helical plasma is a very important issue and required for the reliable design of the helical reactor. In order to contribute to the helical reactor design study, transport characteristics of high temperature plasma have been experimentally investigated in the LHD. This study confirmed that the effects of wall conditioning on the core confinement improvement are attributable to the change of density profile (further peaking of ion heating power profile) and reduction of charge exchange

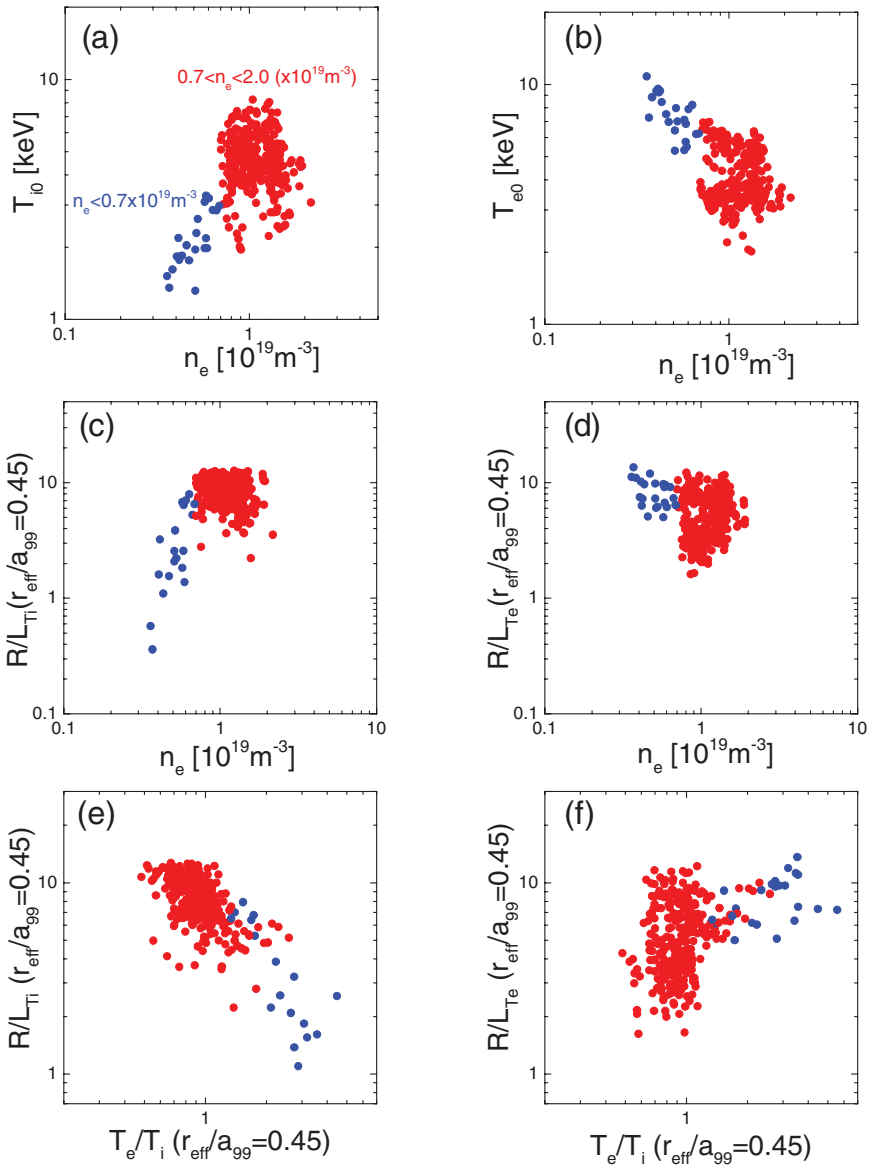

Figure 8. Density dependence of (*a*) central ion temperature and (*b*) electron temperature of the dataset of ITB discharges shown in figure 1. The normalized temperature gradient of the ion and electron ($R/L_{\mathrm{Ti,e}} = -(R/T_{\mathrm{i,e}})$ * grad $T_{\mathrm{i,e}}$,where R is major radius) are shown in (*c*)–(*f*). (*c*) and (*d*) show the density dependence, and (*e*) and (*f*) show the temperature ratio (T_{e} / T_{i}) dependence. The dataset of ITB discharges shown here are obtained with the port through power of $P_{\mathrm{negative\ NBI}} = 10$–16 MW, $P_{\mathrm{positive\ NBI}} = 10$–11 MW and $P_{\mathrm{ECH}} = 0$–2.1 MW. The plasmas with a low density less than $0.7 \times 10^{19}\mathrm{m}^{-3}$ are shown with blue circles in all figures.

loss of energetic ions. The charge exchange loss in the core of reactor relevant plasmas is significantly reduced, and the divertor operation is required to reduce heat load on the divertor plate. In order to investigate the situation, a closed divertor system with vacuum pumping capability is being installed year by year. We will develop a discharge scenario of high performance plasma with divertor operation and a control technique of particle balance in steady state operation, which are important and common issues in both tokamak and helical plasmas.

The combination of ion and electron ITBs and the significant extension of the high temperature regime with $T_{\mathrm{e}} \sim T_{\mathrm{i}}$ have been also demonstrated in this study. The transport improvement in ion heat transport with positive radial electric field may support the high ion temperature scenario with CERC, which is a candidate for the operation scenario in helical reactor plasmas. The ion ITB width is wider than the electron ITB width, indicating the existing different mechanisms of ion transport improvement from CERC. The spatial decoupling of ion and electron ITBs has an advantage to prevent the steep pressure gradient at the barrier from MHD instabilities, which may have some effects on ITB performance in reactor-relevant helical plasma in the future.

The formation of the strong impurity hole was observed in the ion and electron ITB plasmas. The radial position where the density gradient of carbon impurity changes the sign ($r_{\mathrm{eff}}/a_{99} \sim 0.7$) is located round the ion ITB foot position, indicating the impurity transport correlated with the ion heat transport rather than the electron heat transport. The impurity exhaust from the core is an important property for reactor

plasmas and is being studied experimentally [18]. However, further investigation is necessary to understand the physics mechanism of impurity hole formation.

This study demonstrated the integration of ion ITB and electron ITB in helical plasmas, while the collisionality of the presented experiments are still at a lower regime than the collisionality of reactor-relevant helical plasmas. Recently, the collisionality regime in which ITB can be formed is significantly extended toward the high density regime [24]. The integration of ion ITB and electron ITB and the transport characteristics in the higher collisionality regime where, for example, energy equipartition time is comparable to the confinement time, are the next steps of this study. Further studies to explore other improved modes, including the isotope effect, will be also planned in deuterium–deuterium experiments of the LHD.

Acknowledgments

The authors wish to thank all of the engineering staff and operators for their excellent support and operation of the LHD. They also thank Prof H Sugama, Prof S Satake and Prof K Itoh (NIFS), and Dr Y Kamada (JAEA) for their fruitful discussions. This research was supported by NIFS13-KLPR017.

References

[1] Yokoyama M. *et al* 2006 Common features of core electron-root confinement in helical devices *Fusion Sci. Technol.* **50** 327
[2] Fujisawa A. *et al* 2000 Transport barrier formation and bifurcation patterns of potential profiles in the compact helical system heliotron/torsatron *Plasma Phys. Control. Fusion* **42** A103
[3] Maassberg H. *et al* 1997 The neoclassical 'electron-root' feature in W7-AS *Europhys. Conf. Abstracts: 24th Conf. Controlled Fusion and Plasma Physics,* (*Berchtesgaden, Germany, 9–13 June 1997*) vol 21A, part IV 1605
[4] Ida K. *et al* 1998 Formation and termination of high ion temperature mode in heliotron/torsatron plasmas *Phys. Control. Fusion* **40** 793
[5] Takeiri Y. *et al* 2003 Formation of electron internal transport barrier and achievement of high ion temperature in large helical device *Phys. Plasmas* **10** 1788
[6] Castejon F. *et al* 2004 Influence of low-order rational magnetic surfaces on heat transport in TJ-II heliac ECRH plasmas *Nucl. Fusion* **42** 593
[7] Fujisawa A. *et al* 2007 Causal relationship between zonal flow and turbulence in a toroidal Plasma *J. Phys. Soc. Japan* **76** 033501
[8] Ida K. *et al* 2010 Ion internal transport barrier in the large helical device *Contrib. Plasma Phys.* **50** 558
[9] Yokoyama M. *et al* 2008 Extension of the high-ion-temperature regime in the large helical device *Phys. Plasmas* **15** 056111
[10] Nagaoka K. *et al* 2011 Heat and momentum transport of ion internal transport barrier plasmas on the large helical device *Nucl. Fusion* **51** 083022
[11] Takahashi H. *et al* 2013 Extension of the operational regime in high-temperature plasmas and the dynamic-transport characteristics in the LHD *Nucl. Fusion* **53** 073034
[12] Nagaoka K. *et al* 2010 Parameter regime of ion internal transport barrier formation in the large helical device *Plasma Fusion Res.* **5** S2029
[13] Yoshinuma M. *et al* 2010 Charge-exchange spectroscopy with pitch-controlled double-slit fiber bundle on LHD *Fusion Sci. Technol.* **58** 375
[14] Takahashi H. *et al* 2014 High ion temperature plasmas using an ICRF wall-conditioning technique in the large helical device *Plasma Fusion Res.* **9** 1402050
[15] Ido T. *et al* 2006 6 MeV heavy ion beam probe on the large helical device *Rev. Sci. Instrum.* **77** 10F523
[16] Yoshinuma M. *et al* 2009 Observation of an impurity hole in the large helical device *Nucl. Fusion* **49** 062002
[17] Ida K. *et al* 2009 Observation of an impurity hole in a plasma with an ion internal transport barrier in the large helical device *Phys. Plasmas* **16** 056111
[18] Yoshinuma M. *et al* 2015 Abrupt reversal of convective flow of carbon impurity during impurity-hole formation on the LHD *Nucl. Fusion* **55** 083017
[19] Wolf R.C. 2003 Internal transport barriers in tokamak plasmas *Plasma Phys. Control. Fusion* **45** R1
[20] Murakami S. *et al* 2014 Integrated heat transport simulation of high ion temperature plasma of LHD [TH/P6-38] paper presented at the 26th *IAEA Fusion Energy Conf. (St Petersburg, 13–18 October 2014)*
[21] Osakabe M. *et al* 2014 Impact of carbon impurities on the confinement of high-ion-temperature discharges in the large helical device *Plasma Phys. Control. Fusion* **56** 095011
[22] Fujii K. *et al* 2014 Development of a high dynamic range spectroscopic system for observation of neutral hydrogen atom density distribution in large helical device core plasma *Rev. Sci. Instrum.* **85** 023502
[23] Fujii K. *et al* 2015 Study of neutral hydrogen transport in LHD core plasmas based on high dynamic-range Balmer-α spectroscopy *Nucl. Fusion* **55** 063029
[24] Takahashi H. *et al* 2014 Extension of high T_e regime with upgraded electron cyclotron resonance heating system in the large helical device *Phys. Plasmas* **21** 061506
[25] Ida K. *et al* 2009 Dynamics of ion internal transport barrier in LHD heliotron and JT-60U tokamak plasmas *Nucl. Fusion* **49** 095024
[26] Seki R. *et al* 2011 Transport study of LHD high-beta plasmas based on power balance analysis with TASK3D code module *Plasma Fusion Res.* **6** 2402081
[27] Yokoyama M. *et al* 2013 Development of integrated transport analysis suite for LHD plasmas towards transport model validation and increased predictability *Plasma Fusion Res.* **8** 2403016
[28] Beidler C.D. *et al* 1995 A general solution of the ripple-averaged kinetic equation (GSRAKE) *Plasma Phys. Control. Fusion* **37** 463